Monthly Notices of the ROYAL ASTRONOMICAL SOCIETY

MNRAS **534,** 3377–3386 (2024) https://doi.org/10.1093/mnras/stae2308
Advance Access publication 2024 October 08

TRAPUM pulsar and transient search in the Sextans A and B galaxies and discovery of background FRB 20210924D

E. Carli [1]★, L. Levin,[1] B. W. Stappers [1], E. D. Barr [2], R. P. Breton [1], S. Buchner,[3] M. Burgay [4], M. Kramer [2], P. V. Padmanabh [2,5,6], A. Possenti,[4] V. Venkatraman Krishnan [2], S. S. Sridhar[2,7] and J. D. Turner [1]

[1]*Jodrell Bank Centre for Astrophysics, Department of Physics and Astronomy, The University of Manchester, Manchester M13 9PL, UK*
[2]*Max-Planck-Institut für Radioastronomie, Auf dem Hügel 69, D-53121 Bonn, Germany*
[3]*South African Radio Astronomy Observatory (SARAO), 2 Fir Street, Black River Park, Observatory, Cape Town 7925, South Africa*
[4]*INAF-Osservatorio Astronomico di Cagliari, via della Scienza 5, I-09047 Selargius, Italy*
[5]*Max-Planck-Institut für Gravitationsphysik (Albert-Einstein-Institut), D-30167 Hannover, Germany*
[6]*Leibniz Universität Hannover, D-30167 Hannover, Germany*
[7]*SKA Observatory, Jodrell Bank, Lower Withington, Macclesfield SK11 9FT, UK*

Accepted 2024 September 30. Received 2024 September 28; in original form 2024 June 4

ABSTRACT

The Small and Large Magellanic Clouds are the only galaxies outside our own in which radio pulsars have been discovered to date. The sensitivity of the MeerKAT radio interferometer offers an opportunity to search for a population of more distant extragalactic pulsars. The TRAPUM (TRansients And PUlsars with MeerKAT) collaboration has performed a radio-domain search for pulsars and transients in the dwarf star-forming galaxies Sextans A and B, situated at the edge of the Local Group 1.4 Mpc away. We conducted three 2-h multibeam observations at *L* band (856–1712 MHz) with the full array of MeerKAT. No pulsars were found down to a radio pseudo-luminosity upper limit of 7.9±0.4 Jy kpc^2 at 1400 MHz, which is 28 times more sensitive than the previous limit from the Murriyang telescope. This luminosity is 30 per cent greater than that of the brightest known radio pulsar and sets a cut-off on the luminosity distributions of the entire Sextans A and B galaxies for unobscured radio pulsars beamed in our direction. A fast radio burst was detected in one of the Sextans A observations at a dispersion measure (DM) of 737 pc cm^{-3}. We believe this is a background event not associated with the dwarf galaxy due to its large DM and its signal-to-noise ratio being strongest in the wide-field incoherent beam of MeerKAT.

Key words: stars: neutron – pulsars: general – galaxies: individual: Sextans A, Sextans B – Local Group – fast radio bursts – radio continuum: transients.

1 INTRODUCTION

The Small and Large Magellanic Clouds (SMCs and LMCs) are the only galaxies outside the Milky Way in which radio pulsars have been discovered to date (Titus et al. 2019; Hisano et al. 2022, and references therein) due to their proximity and position away from the Galactic plane. Of the nearly 3400 radio pulsars that have been discovered, only 31 are extragalactic [see the Australia Telescope National Facility (ATNF) pulsar catalogue for a list, Manchester et al. 2005]. So far, no rotation-powered pulsars have been found at distances larger than that of the SMC (60 kpc; Karachentsev et al. 2004). Extragalactic pulsars are sought after for insights on the influence of different galactic properties on neutron star (NS) formation. For example, the impact of galactic metallicity and star formation history on stellar mass and supernova physics can be investigated (Heger et al. 2003; Titus et al. 2020). A rotation-powered pulsar outside the Magellanic Clouds would extend these studies to a new galaxy.

Sextans A and B are dwarf irregular faint galaxies at the edge of the Local Group, 1.4 Mpc away (Dalcanton et al. 2009), and no pulsars are known within 3 deg of their location (Manchester et al. 2005). They are 260 kpc away from each other (Dohm-Palmer et al. 1997), with sizes of about 4 kpc (Bellazzini et al. 2014). The expected Milky Way dispersion measure (DM) contribution in their direction is low: about 32 or 45 pc cm^{-3} according to the YMW2016 or NE2001 electron density models, respectively (Cordes & Lazio 2004; Yao, Manchester & Wang 2017). This is of the same order of magnitude as the DM contributions in the direction of the Magellanic Clouds and is favourable to radio pulsar searches.

The galaxies are undergoing episodes of more intense star formation, which started 50 Myr ago in Sextans A (Dohm-Palmer et al. 1997) and 1–2 Gyr ago in Sextans B (Sakai, Madore & Freedman 1997). Both are still star-forming at the rate of 2–8 $\times 10^{-3} M_\odot$ yr^{-1} (Weisz et al. 2011). This can lead to the presence of young pulsars

★ E-mail: ecarli@swin.edu.au

like it has in the Magellanic Clouds[1] (e.g. Seward, Harnden & Helfand 1984; Lamb et al. 2002; Maitra et al. 2021; Carli et al. 2024), and an abundance of young systems per unit mass compared to the Milky Way (e.g Maggi et al. 2019). The discovery of young pulsars is scientifically interesting. Among them, magnetars (which have the highest known stellar magnetic fields) are important for a variety of fundamental physics and astrophysics investigations (Esposito, Rea & Israel 2021), including as one of the progenitors of fast radio bursts (FRBs; Platts et al. 2019; Bochenek et al. 2020). One extragalactic magnetar has been discovered in each of the Magellanic Clouds (Helfand & Long 1979; Lamb et al. 2002); giant magnetar flares have been observed in nearby galaxies (Mereghetti et al. 2024; Trigg et al. 2024); and an FRB repeater has been found in a dwarf galaxy (Tendulkar et al. 2017): the powerful emission from these exotic systems can be detected at extragalactic distances. Additionally, young pulsars can emit giant narrow pulses (e.g. the extragalactic Crab pulsar twin in the LMC, Johnston & Romani 2003). If a pulsar is too distant and thus too faint to be detected even in a long integration, single pulses that are orders of magnitude stronger than average may still be detected individually, although distance is still a challenge (see Section 6). Sextans A and B host multiple shell-like structures formed as the result of photoionization from massive stars, stellar winds, and supernovae. Each galaxy contains three candidate supernova remnants (Gerasimov et al. 2022, 2024). There is also one supernova remnant identified in X-rays in Sextans A (Kappes 2005). These can potentially host young pulsars.

Low metallicity can strongly decrease stellar mass-loss rates through line-driven winds in progenitor stars and thus increase the mass of the final remnant. This can lead to an increased NS birth rate, and, possibly, increased NS masses (Heger et al. 2003). Sextans A and B have a lower metallicity[2] than the Magellanic Clouds (Garcia et al. 2019) and the Milky Way, therefore many scientifically valuable compact objects might be formed (e.g. Titus et al. 2020). For example, the low-metallicity SMC hosts a 50 times higher density of high-mass X-ray binary systems (a high-mass star in a binary with an NS or black hole) than in the Milky Way (Haberl & Sturm 2016; Yang et al. 2017). High-mass systems that have not yet reached their final evolutionary stages are known in Sextans A under the form of a large population of early O-type stars (Garcia et al. 2019; Lorenzo et al. 2022) and accreting X-ray binaries (Kappes 2005). This is indicative of systems that will form or contain NSs and recycled pulsars.

Finally, old star clusters are a prime target to search for millisecond (MSPs) and binary pulsars (see Lorimer 2008), as well as transients: an FRB was pinpointed to a globular cluster (GC) 3.7 Mpc away in the galaxy M81 (twice the distance to the Sextans galaxies), which was until then an ill-favoured progenitor environment (Bhardwaj et al. 2021; Kirsten et al. 2022; Kremer et al. 2023). A low-metallicity, 9 Gyr GC is already known in Sextans A (Beasley et al. 2019; Gvozdenko et al. 2024). Besides this, Sextans B hosts a 1–3 Gyr star cluster (Sharina, Puzia & Krylatyh 2007). Both these clusters could potentially harbour multiple millisecond pulsars.

TRAPUM (TRAnsients and PUlsars with MeerKAT) is a Large Survey Project of the MeerKAT telescope (trapum.org, Stappers & Kramer 2016). The collaboration has already discovered over 200 pulsars.[3] One of TRAPUM's science goals is to find new extragalactic pulsars. Motivated by the sensitivity of the MeerKAT telescope to faint, distant pulsars (as evidenced by recent discoveries in the SMC, see Carli et al. 2024) and new transients, we have conducted observations of the Sextans A and B galaxies. The observations, described in Section 2, encompass the whole galaxies and thus their entire pulsar population with favourable viewing geometries, which as detailed above could be rich in interesting systems. We detail our search analysis in Section 3, and report the detection of an FRB in Section 4, likely originating from outside the targeted dwarf galaxy. We state our upper limits on radio pulsations from these galaxies in Section 5. Considering the distance to these galaxies being 23 times larger than the distance to the Magellanic Clouds, we discuss what systems could be detected in Section 6.

2 OBSERVATIONS

A detailed introduction to TRAPUM's observing strategy for nearby galaxies with MeerKAT is presented in Carli et al. (2024). We conducted three 2-h multibeam observations of the dwarf galaxies Sextans A and B. For each observation, a tiling of coherent beams was placed at the centre of the pointing [i.e. at the centre of the MeerKAT primary incoherent beam that has a full width at half-maximum (FWHM) of about 1 deg at *L* band]. The pointings were aimed at the centre of each galaxy. We used the TRAPUM backends Filterbanking Beamformer User Supplied Equipment (FBFUSE) and Accelerated Pulsar Search User Supplied Equipment (APSUSE) to synthesize and record about 260 beams as filterbank search-mode files (Chen et al. 2021; Padmanabh et al. 2023). We carried out the observations at *L* band (856–1712 MHz), with 2048 frequency channels and a sampling time of 153 μs. The beams were formed using the MeerKAT full array (56 to 60 antennas out of 64 due to availability) with a maximum baseline length of about 8 km. Sextans A and B are small sources, with a diameter of about 5–6 arcmin (Bellazzini et al. 2014). Despite the much reduced beam size of the full array of MeerKAT compared to its core configuration, we were able to cover each entire galaxy with about 260 beams and comply with APSUSE data rate recording requirements. This allowed us to obtain the best sensitivity for our integration time. The characteristics of the individual observations are given in Tables 1 and 2. In Figs 1 and 2, we show the layout of the MeerKAT coherent beams for each observation. The beam positions were retrieved from the FBFUSE record of the observation. A high-resolution coherent beam point spread function (PSF) was simulated with MOSAIC (Chen et al. 2021) at the centre coordinates of the pointing, at the central time of the observation, with the antennas used during the observation and at the central frequency of *L* band. The ellipse-shaped beam contours, fitted by MOSAIC to the PSF, are shown at the sensitivity overlap of the tiling. One 2-h pass on both sources occupies around 50 terabytes of disc space on the APSUSE cluster.

Imaging data were recorded commensally for each observation as correlated visibilities with the full array. The visibility data were correlated in the 'wideband coarse (4k)' mode, resulting in 4096 208.98 kHz-wide channels to cover the 856–1712 MHz frequency range. The time resolution of the visibility data is 8s.

[1]There was a recent episode of stellar formation in the SMC about 40 Myr ago (Harris & Zaritsky 2004), and in the LMC 12 Myr ago (Harris & Zaritsky 2009).

[2]The mean [Fe/H] values are, from lowest to highest metallicity: −1.6 for Sextans B, −1.5 for Sextans A (Bellazzini et al. 2014), −0.7 for the SMC, −0.3 for the LMC (Luck et al. 1998), and about 0 for the Milky Way (e.g. Hayden et al. 2014).

[3]http://trapum.org/discoveries/

Table 1. The Sextans A observation parameters. For each observation, a tiling of coherent beams is placed at the centre of the pointing, within the MeerKAT primary incoherent beam. The pointing is aimed at the centre of the Sextans A galaxy: RA(J2000) = $10^{h}11^{m}00\overset{s}{.}5$ Dec.(J2000) = $-04°41'30\overset{''}{.}0$ (Paturel et al. 2003). The coherent beam semi-axes, fitted by MOSAIC, are given in arcseconds in the right ascension and declination directions, with the ellipse position angle (taken clockwise from North).

Date	Observation length	Number of incoherent antennas	Number of coherent antennas	Number of coherent beams	Coherent beam tiling sensitivity overlap	Coherent beam size (50 per cent sensitivity)
2021 June	6798 s	57	56	246	47 per cent	$26\overset{''}{.}2$ $9\overset{''}{.}9$ $-34\overset{°}{.}1$
2021 July	7167 s	62	60	260	50 per cent	$15\overset{''}{.}0$ $10\overset{''}{.}1$ $55\overset{°}{.}6$
2021 September	7085 s	62	60	260	50 per cent	$19\overset{''}{.}6$ $12\overset{''}{.}3$ $62\overset{°}{.}9$

Table 2. The Sextans B observation parameters. For each observation, a tiling of coherent beams was placed at the centre of the pointing, within the MeerKAT primary incoherent beam. The pointing was aimed at the centre of the Sextans B galaxy: RA(J2000) = $10^{h}00^{m}00\overset{s}{.}82$ Dec.(J2000) = $05°20'09\overset{''}{.}57$. The coherent beam major axes, fitted by MOSAIC, are given in arcseconds in the right ascension and declination directions, with the ellipse position angle (taken clockwise from North). The overlaps obtained may be different than intended due to updates to FBFUSE and the MOSAIC software, see Carli et al. (2024) for more details.

Date	Observation length	Number of incoherent antennas	Number of coherent antennas	Number of coherent beams	Coherent beam tiling sensitivity overlap	Coherent beam size (50 per cent sensitivity)
2021 June	7156 s	57	56	266	50 per cent	$17\overset{''}{.}9$ $10\overset{''}{.}8$ $-39\overset{°}{.}1$
2021 July	7152 s	62	60	252	50 per cent	$14\overset{''}{.}9$ $8\overset{''}{.}2$ $76\overset{°}{.}1$
2021 September	6540 s	62	60	252	50 per cent	$19\overset{''}{.}6$ $9\overset{''}{.}9$ $76\overset{°}{.}2$

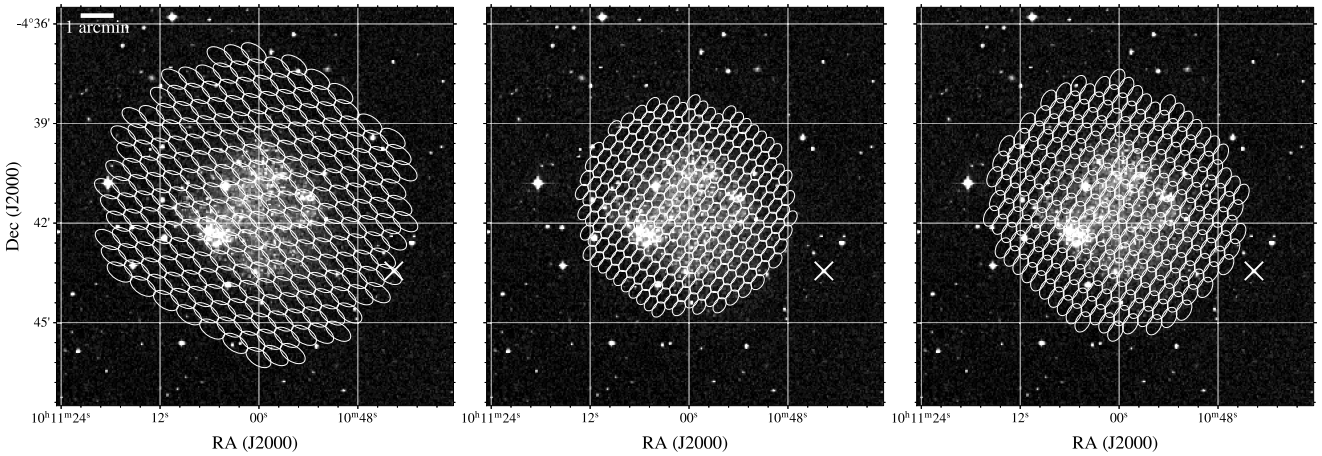

Figure 1. The three observations of Sextans A (first to third pass left to right) are displayed over a DSS image (Space Telescope Science Institute 1995). The observed MeerKAT full array coherent beams are shown at 50 per cent sensitivity (47 per cent for the first pass) as white ellipses, simulated with MOSAIC. The MeerKAT incoherent beam size is larger than the figure with an FWHM of about 1 deg at *L* band. This figure was generated with the ⟨0:sc ⟩aplpy⟨/0:sc⟩ Python package. The GC (Beasley et al. 2019) is shown with a cross. The beam orientation changes are due to the source being observed when rising in the first pass and setting in the two other passes. The beam size depends on the hour angle of the source and the location of the antennas used.

3 DATA REDUCTION

The data were processed locally, on the APSUSE computing cluster via the standard TRAPUM search pipeline (see Section 6.1 in Padmanabh et al. 2023). We first processed the survey data with a periodicity search pipeline. Radio frequency interference (RFI) cleaning was performed for the first two passes with a combination of IQRM (Morello, Rajwade & Stappers 2021), and a multibeam RFI filter MULTITRAPUM.[4] The latter is a wrapper of `rfifind` which removes signals detected in several beams with sufficient spatial separation. We switched to PULSARX's `filtool` (Men et al. 2023) for the third pass as part of a TRAPUM pipeline upgrade, where we also applied a standard channel mask. A de-dispersion plan was computed with PRESTO's `DDplan.py` script. The DM step sizes (i.e. the DM increment between each of the trial DMs) and sampling time are increased to match the growth of channel time smearing at higher DMs, to avoid unnecessarily high time resolution and thus spurious computation. We used the DEDISP library (Barsdell et al. 2012; Levin 2012) for dedispersion over DMs up to 500 pc cm^{-3} (where 1 ms of combined intra-channel dispersion and de-dispersion step size smearing is reached) as part of the PEASOUP suite, a GPU-based pulsar searching software (Morello et al. 2019; Barr 2020; Sengar et al. 2023). The 2-h long data were not corrected for acceleration before performing a fast Fourier transform (FFT) search using PEASOUP.

[4] https://github.com/mcbernadich/multiTRAPUM by Miquel Colom i Bernadich

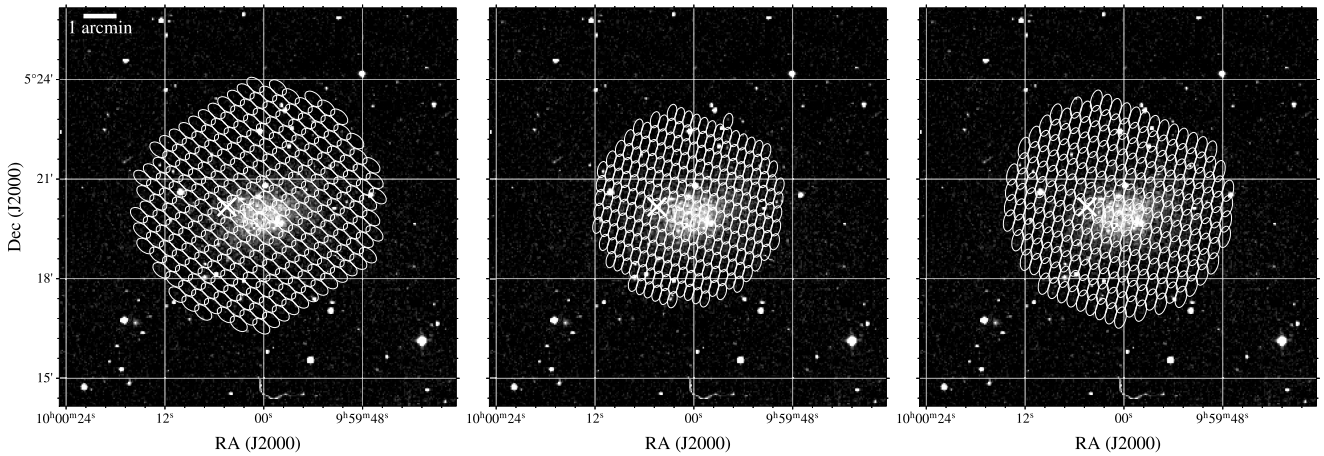

Figure 2. The three observations of Sextans B (first to third pass left to right) are displayed over a DSS image. The MeerKAT incoherent beam size is larger than the figure. The observed MeerKAT full array coherent beams are shown at 50 per cent sensitivity as white ellipses, simulated with MOSAIC. This figure was generated with the ⟨0:sc ⟩aplpy⟨/0:sc⟩ Python package. The star cluster (Sharina et al. 2007) is shown with a cross. The beam orientation changes are due to the source being observed when rising in the first pass and setting in the two other passes. The beam size depends on the hour angle of the source and the location of the antennas used.

Thus, we searched for systems with no significant[5] acceleration from a binary companion, with a minimum FFT spectrum signal-to-noise ratio (S/N) of 8 and a maximum period of 10 s. The 2-h time series were zero-padded to the next nearest power of 2, 2^{26}, resulting in a better resolved Fourier spectrum. Candidates were harmonically summed by PEASOUP up to the eighth harmonic (Taylor & Huguenin 1969). The resulting spectral candidates were then sifted by PEASOUP, i.e. clustered in DM, period and harmonics, in each beam independently. A list of common local RFI fluctuation frequencies was removed from the searches. This returned on average around 2000 candidates in one coherent beam for one observation.

This was followed by multibeam spatial sifting,[6] which uses the expected spatial relationship of real sources to identify RFI (Padmanabh et al. 2023), after which less than 200 candidates remained in one beam for one observation. We note that a recently discovered bug in the multibeam filtering code overremoved candidates from an in-built list of RFI fluctuation frequencies. It is possible to retroactively check if a specific candidate has been removed in a list stored as a data product of this pipeline. We only kept candidates with periods longer than eight time samples (1.225 ms), which typically removed a few candidates per beam in each observation. We folded the raw data with the parameters of the filtered FFT candidates using PULSARX's `psrfold_fil` (Men et al. 2023), which downsamples the raw timeseries into folded data as follows: 64 time samples (bins) per candidate pulse profile (128 for signals with $P > 100$ ms), each sub-integration of the observation in time is 20 s long, and the number of frequency channels is reduced to 64. `psrfold_fil` cleans the full resolution data from RFI with `filtool` before folding and applies the CLFD RFI removal software (Morello 2023) on the folded data. The folds were optimized to the highest S/N pulse profile over a period and period derivative range around the PEASOUP-detected topocentric spin frequency so that the maximum smearing is one pulse period over the whole observation time, and over a DM range so that the maximum dispersion delay is one pulse period over the whole bandwidth.

We then partially classified the folded candidates with PICS [a pulsar image-based classification system based on machine learning (Zhu et al. 2014)]. We used a minimum score of 10 per cent pulsar-like for both the original PALFA model (Zhu et al. 2014) and TRAPUM models (Padmanabh et al. 2023), as well as a minimum folded profile S/N of 7 to eliminate candidates. This returned on average less than one candidate per beam for each observation to classify visually. We used a Graphical User Interface candidate classifier tool, CANDYJAR,[7] to classify the folded candidate plots by eye. Two or three viewers classified the candidates, most of which were consistent with RFI or noise, except for about five candidates per observation of each galaxy which were low confidence pulsar candidates. These were cross-checked between the first and second pass observations, and their discovery positions re-observed in the third pass. None were detected and classified as pulsar candidates more than once, and we hence discarded them as candidates arising from noise fluctuations.

We also searched the full observations for single pulses with TRANSIENTX (Men & Barr 2024) on the data downsampled by a factor of 2 in time to a sampling time of 306 μs, RFI cleaned by a `rfifind` channel mask and PULSARX's `filtool`. We used a 100 ms maximum search width over DMs 0 to 5000 pc cm^{-3} and a minimum single pulse S/N of 8. On average, several hundred candidates per observation were returned, most of which came from the incoherent beam that is more affected by RFI due to its wide field of view. A visual inspection of all the single pulse candidates indicated they were mostly consistent with RFI or noise, except for less than five candidates per observation of each galaxy which were low-confidence candidates (see Fig. 3), and one FRB discovery described in the next section. The low-confidence candidates were cross-checked between the three passes with no redetections, suggesting they could have arisen from noise fluctuations. As the raw data were too voluminous to keep, we stored an RFI-cleaned (by IQRM) downsampled (512 channels and 1.225 ms sampling time)

[5]Systems with low acceleration and long orbital periods can be detected, as long as the change in spin frequency is small compared to the frequency resolution of the FFT search (see e.g. Johnston & Kulkarni 1991).
[6]https://github.com/prajwalvp/candidate_filter by Lars Künkel

[7]https://github.com/vivekvenkris/CandyJar by Vivek Venkatraman Krishnan

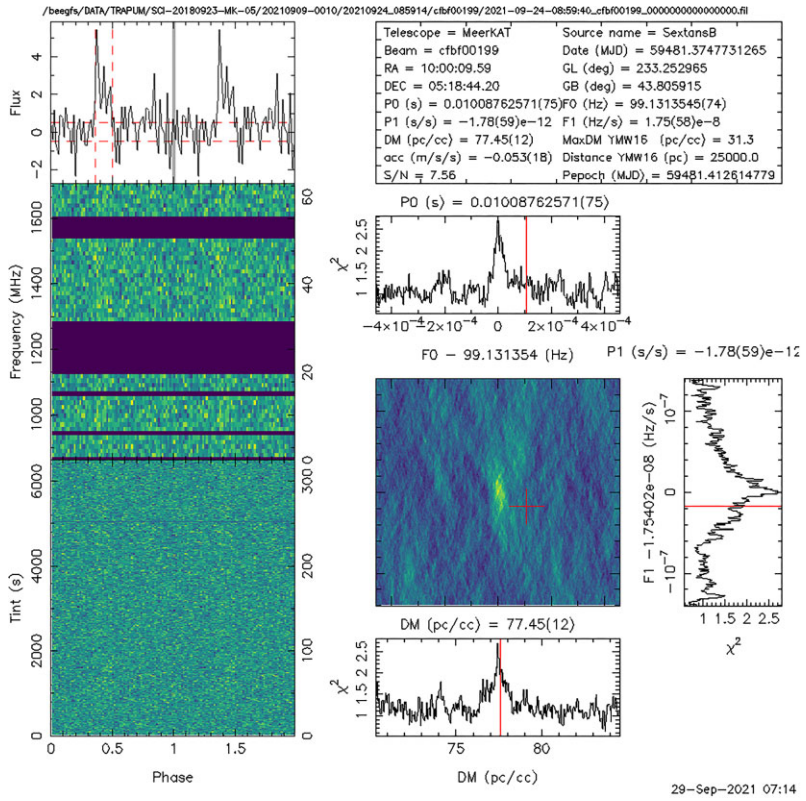

Figure 3. An example of a low-confidence candidate from this survey, from the third pass observation of Sextans B. Details of the PULSARX folding package can be found in Men et al. (2023).

version of the second and third passes. Apart from the offline processing using TRANSIENTX, a commensal search for transients was carried out on the incoherent beam and coherent beams using the MeerTRAP backend TUSE (Transient User Supplied Equipment). The capabilities and pipelines for MeerTRAP are described in Rajwade et al. (2022).

4 FRB 20210924D

Two transient candidates from the third pass Sextans A observation matched in date (2021-09-24 11:59:50.98 UTC, MJD 59481.49989563), width (about 1 ms), and DM (737 pc cm^{-3}). One was detected by the pipeline in a coherent beam (CB, number `000175`) at location RA(J2000) = $10^{\rm h}10^{\rm m}59\overset{\rm s}{.}71$ Dec(J2000) $=-04^{\circ}39'08\overset{''}{.}20$ with an S/N of 9.2 and the other in the incoherent beam (IB) centred on Sextans A with an S/N of 15.7. Inspection of the raw data revealed that bright narrow-band emission from the transient had been partially masked by the `filtool` RFI mitigation (as expected), lowering its S/N; and that the pulse was present in many CBs with a lower S/N than in the IB.[8] This suggests that the transient occurred in the IB outside the coherent tiling, and was detected in the sidelobes of the CBs. The short-duration transient is consistent with an FRB due to its high DM. The narrow-band nature of this FRB could be due to the beam response (e.g. if the FRB is located in an incoherent beam sidelobe, Obrocka 2015) or an intrinsic feature of the emission (Xu et al. 2022). Fainter emission is visible throughout the band (see Fig. 4). We found no published previous occurrences of this FRB and indeed no known FRBs within 7 deg of Sextans A.[9] We show the incoherent beam detection in Fig. 4 and the strongest coherent beam detection in Fig. 5. We used the software SCATFIT (Jankowski 2022; Jankowski et al. 2023) to evaluate the properties of the FRB from the IB data, which we present in Table 3. Scattering parameters could not be disentangled from dispersion effects, either due to weak scattering or the low S/N of the FRB at high frequencies.

We attempted to localize the FRB by locating a transient source in the correlated visibility data obtained commensally in the third pass Sextans A observation (see Section 2, schedule block number `20210909-0010`). We performed this by subtracting all the persistent continuum sources from the visibility data and searching for residual emission in a single time cell corresponding to the time stamp when the FRB was detected in the IB and CBs. We limited our search to a small bandwidth of about 12 MHz centred at 1468 MHz since this frequency range contains the dominant emission in the incoherent and coherent beams.

The narrow-band visibility data, with a scan length of 2 h and a time resolution of 8 s, were calibrated following the standard procedure using the COMMON ASTRONOMY SOFTWARE APPLICATIONS (CASA; The CASA Team 2022) package. Automated RFI flagging, usually part of the standard calibration workflow of interferometry data, was not performed on the Sextans A data to avoid inadvertent removal of the FRB signal. Manual RFI removal was performed instead. Next, we imaged the entire 2-h observing block except for the single

[8]The S/N post-`filtool` RFI cleaning was below the S/N=8 threshold for detection by our pipeline in all coherent beams but one. Therefore, the coherent beam with the strongest S/N was the only pipeline detection in the tiling.

[9]Using the Transient Name Server, https://www.wis-tns.org/. The FRB report for this publication is available here.

Table 3. The properties of FRB 20210924D as fitted by SCATFIT on the incoherent beam data, where W_{eq} is the equivalent width of the pulse and W_{50} is the width of the burst at 50 per cent of the peak intensity.

Band name	Central frequency (MHz)	Fluence (Jy ms)	W_{eq} (ms)	W_{50} (ms)
Upper half	1497.8	0.83(4)	0.74(5)	0.65(4)
Lower half	1069.8	1.3(2)	1.9(6)	1.6(3)
Whole *L* band	1283.8	0.90(7)	0.86(9)	0.65(8)

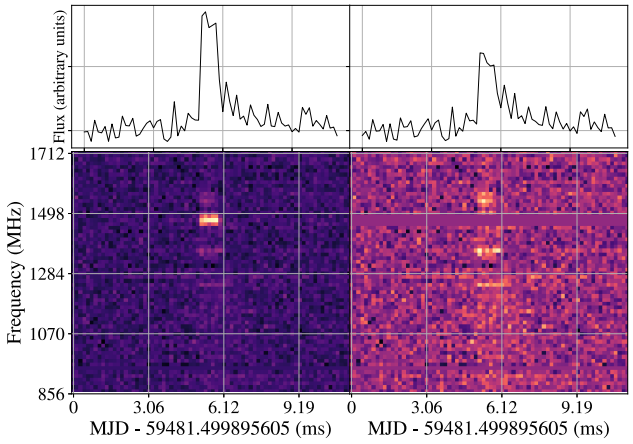

Figure 4. The detection of FRB 20210924D in the incoherent beam of the third pass of Sextans A. In the bottom left plot, we show the dynamic spectrum of the FRB in the *L* band of MeerKAT reduced to 64 subbands (from a recorded frequency resolution of 2048 channels) where RFI has been removed manually with PSRCHIVE. The time resolution is the sampling time: 153 μs. In the bottom right plot, we show the same dynamic spectrum with the three subbands that contain the brightest narrowband emission of the FRB removed. This makes the fainter emission more perceptible. The top plots are the total flux added in frequency. TRANSIENTX evaluates the S/N of the burst in the left panel as 30.9 and its DM as 737.54 ± 0.61.

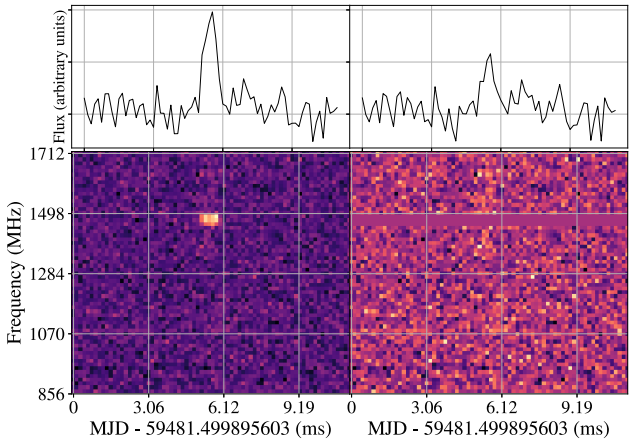

Figure 5. The strongest detection of FRB 20210924D in a coherent beam of the third pass of Sextans A. The plot is as described in Fig. 4. The S/N of the burst in the left panel (as evaluated by TRANSIENTX) is 13.1.

8 s time cell where the FRB signal might be present (we ensured the FRB was not dispersed beyond a single time cell). Ignoring the single time cell ensures that the FRB signal is not accidentally subtracted from the visibility data. We then generated a model of sources in the continuum image using the PYBDSF source finder (Mohan & Rafferty 2015). We subtracted the generated model from the visibility

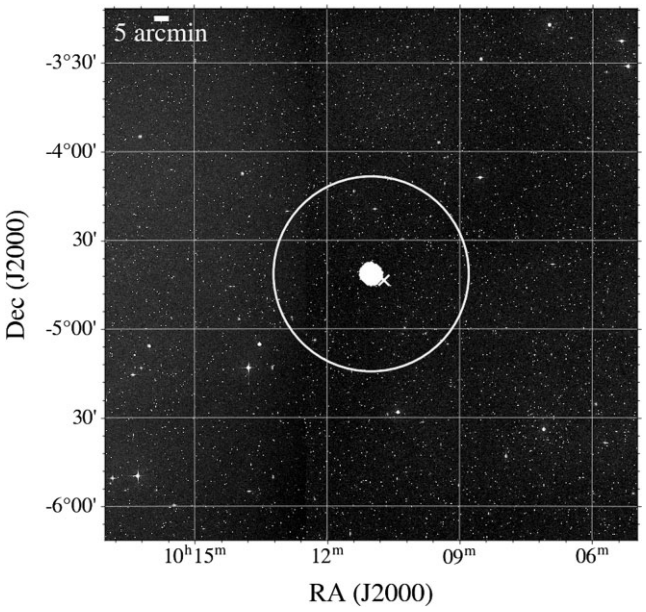

Figure 6. The beams recorded in the third pass observation of Sextans A are displayed over a DSS image. The large circle is the MeerKAT incoherent beam size at half-maximum sensitivity at the centre frequency of *L* band. The GC (Beasley et al. 2019) is shown with a cross. The observed MeerKAT full array coherent beams are shown at 50 per cent sensitivity as white ellipses, simulated with MOSAIC (Chen et al. 2021). This figure was generated with the ⟨0:sc ⟩aplpy⟨/0:sc⟩ Python package.

data, which should only contain any remaining transient emission. We imaged the residual visibility data to produce a 5° × 5° image. Searching the residual image visually and using the PYBDSF source finder yielded no detection, thus we were not able to identify the FRB in the image. The third pass image of Sextans A was generated from 62 antennas. Using the relationship between imaged and time-domain significance from Rajwade et al. (2022), we expect that the transient source would have an S/N of about 3–4 in an 8 s-integrated image, which may explain this non-detection.

The sky position of the FRB is thus unconstrained. The MeerKAT incoherent beam has a FWHM of 1.1 deg at the centre frequency of *L* band and 0.9 deg at the highest frequency of the band (Asad et al. 2021), and the source could be far from the pointing centre, in a less sensitive area of the IB. We show the IB size relative to the coherent beam tiling in Fig. 6.

5 SENSITIVITY LIMITS

We calculate radio flux density sensitivity limits using the the radiometer equation (equation 1) applied to pulsar observations (p. 265 Lorimer & Kramer 2005) with the usual simplification of a

Table 4. Survey sensitivity calculations parameters for our observations with the *L*-band receiver of MeerKAT (Bailes et al. 2020). The digitization correction factor is taken from Kouwenhoven & Voûte (2001).

Parameter	Value
Bandwidth $\Delta\nu$ (MHz)	856
Centre frequency ν (MHz)	1284
System temperature $T_{\rm sys}$ (K)	18
Sky temperature $T_{\rm sky}$ (K)	6.5
Gain G (60 coherent antennas, K Jy^{-1})	2.625
Gain G (62 incoherent antennas, K Jy^{-1})	0.344
Number of frequency channels	2048
Sampling time (μs)	153
Number of polarizations recorded $n_{\rm pol}$	2
Digitization correction factor β (8 bit)	1.0

constant sensitivity across the bandwidth and a flat pulsar spectrum:

$$S_{\rm min} = \frac{\rm S/N_{min} \times (T_{sys} + T_{sky}) \times \beta}{\epsilon \times G \times \sqrt{n_{\rm pol} \times t_{\rm obs} \times \Delta\nu}} \times \sqrt{\frac{\delta}{1-\delta}}. \quad (1)$$

We use the parameters detailed in Table 4 for MeerKAT in a full array configuration with 60 coherent antennas at *L* band at the centre of the pointing (primary beam location), and at the centre of a coherent beam (where it has maximum sensitivity). Other parameters used in our sensitivity calculations are given in Table 5. We use an FFT efficiency factor $\epsilon = 0.7$ to perform a spectral to folded S/N conversion (Morello et al. 2019). Thus, a minimum S/N cut of 8 in the FFT corresponds to a folded S/N of approximately 12. For a pulsar with a rotation period of 100 ms, this yields a flux density limit of $S_{1284\,\rm MHz} = 4.8\,\mu$Jy. At shorter periods, pulse widening due to sampling time, dispersion smearing in a frequency channel (p. 109 Lorimer & Kramer 2005), and dispersion scattering (Lewandowski, Kowalińska & Kijak 2015) are introduced. Due to these effects, at shorter periods, the duty cycle δ departs from our assumed intrinsic 2.5 per cent value[10] (Fig. 7), increasing the flux density limit to 14 μJy at 1.225 ms. The sensitivity reduction for a coherent beam placed at the edge of the optical extent of the dwarf galaxy is less than 1 per cent (using a primary beam sensitivity model based on Asad et al. 2021). We can also provide a limit for the Sextans A GC in the first pass observation, accounting for factors that caused the sensitivity to be decreased, i.e. the reduced number of antennas, the position in the incoherent beam and in the coherent beam: 7, 1, and 50 per cent sensitivity reductions, respectively. For a pulsar with a rotation period of 1.225 ms (including pulse broadening) this yields a flux density limit of $S_{\rm GC,1284\,MHz,MSP} = 23\,\mu$Jy for the Sextans A GC.

In Fig. 7, we show the sensitivities of all pulsar surveys that have observed Sextans A: this work, the Parkes Southern pulsar survey (Manchester et al. 1996), the Parkes high-latitude pulsar survey (Burgay et al. 2006), the High Time Resolution Universe Pulsar Survey (HTRU Keith et al. 2010), the Green Bank telescope 350 Mhz drift-scan survey (Boyles et al. 2013; Lynch et al. 2013), and the Parkes Survey for Pulsars and Extragalactic Radio Bursts (SUPERB Keane et al. 2018). Again, we use the the radiometer equation applied to pulsar observations (equation 1) to calculate

[10]This value of δ is the median intrinsic duty cycle from the ATNF pulsar catalogue, for radio-emitting pulsars with a measured pulse width, excluding GC pulsars, MSPs, rapidly rotating radio transients, magnetars and binary pulsars.

Table 5. Survey sensitivity calculations parameters. The sky temperature was retrieved from Zheng et al. (2017) using PYGSM (Price 2016).

Parameter	Value
Assumed pulsar duty cycle δ (per cent)	2.5
Minimum spectral S/N searched to S/N$_{\rm min}$	8
FFT efficiency factor ϵ	0.7
Observation time $t_{\rm obs}$	7200 s

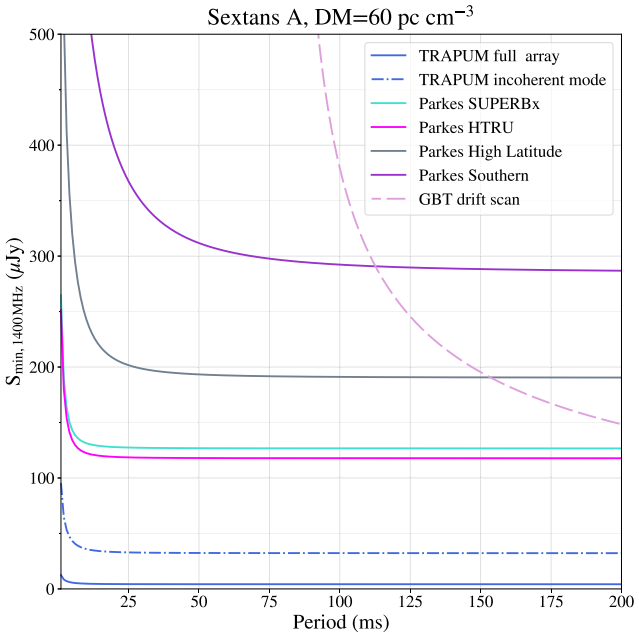

Figure 7. Flux density sensitivity limits as a function of pulsar period for all pulsar surveys that have observed Sextans A. The maximum period searched by our survey is 10 s: we have shown here the shortest periods in order to indicate where our sensitivity deviates from being quasi-constant as a function of period.

their flux density sensitivity limits. We find the values of the parameters listed in Table 4 for the surveys in their respective papers, including their minimum S/N, except for duty cycle which we set at 2.5 per cent, and sky temperature. We compute the latter at each survey's central frequency with PYGSM (Price 2016). We assume the gain of Murriyang to be 0.735 K Jy^{-1} in all cases, using the boresight value (Manchester et al. 2001). The digitization correction factors are taken from Kouwenhoven & Voûte (2001): 1.0 for 8-bit digitization, 1.25 for 1-bit, and 1.06 for 2-bit. We rescale all surveys to 1400 MHz assuming a -1.60 pulsar spectral index (Jankowski et al. 2018). We note that the Parkes Southern pulsar surveyand the Green Bank telescope drift-scan survey have central frequencies of 436 and 350 MHz, respectively. This means that the spectral index conversion is speculative as there is a range of pulsar spectral indices that may vary the resulting sensitivity. Other surveys compared were all conducted at *L* band, close to a central frequency of 1400 MHz. We use the highest DM that has been searched by all the surveys, 60 pc cm^{-3}. We again take into account pulse widening effects as detailed previously. Temperature contributions from the ground and the atmosphere, scintillation effects, effective bandwidth (due to RFI masking and band characteristics), de-dispersion step size, and harmonic summing contributions are not taken into account. As shown in Fig. 7, our radio flux density limit rescaled at 1400 MHz

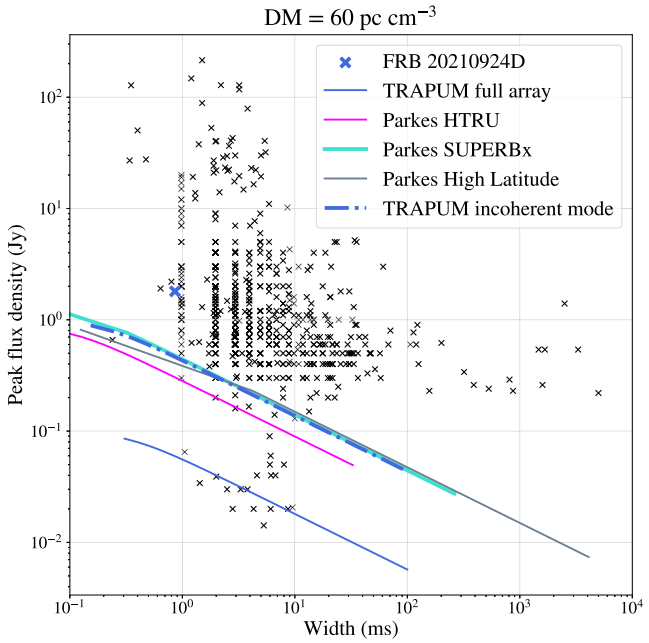

Figure 8. Flux density sensitivity limits of all *L*-band surveys that have performed a targeted search for transient dispersed pulses from Sextans A. Known FRBs are plotted as black crosses, from the FRBSTATS catalogue. We note that the catalogued FRB flux densities are calculated with varying methods and should be treated as an approximation. Indeed, the true flux density of FRB 20210924D is unknown due to its unknown position in the incoherent beam sensitivity response. The quantization of FRB values is due to rounding and sampling time limitations.

for the mean spectral index is $S_{1400\,\mathrm{MHz}} = 4.2\pm0.2\,\mu$Jy at the centre of the pointing, for a pulsar with a rotation period of 100 ms. This 1400 MHz flux density limit is 28 times more sensitive than the best previous flux density limit from Keith et al. (2010). Sextans B has been observed by the same surveys except HTRU, and has a similar sky temperature, and thus similar flux limits.

A limiting single pulse flux density sensitivity plot of transient searches of Sextans A is shown in Fig. 8. All *L*-band surveys mentioned earlier except Parkes Southern have searched for dispersed single pulses: the Parkes high-latitude pulsar survey (Rane et al. 2016), the High Time Resolution Universe Pulsar Survey (Burke-Spolaor et al. 2011), and the Parkes Survey for Pulsars and Extragalactic Radio Bursts (SUPERB Keane et al. 2018). We do not compare with the Green Bank telescope 350 MHz drift-scan survey (Boyles et al. 2013; Lynch et al. 2013) or CHIME (The CHIME/FRB Collaboration 2018) due to the difference in observed frequency. We find the values of the parameters listed in Table 4 for the surveys in their respective papers, and the same assumptions as before. We also use the minimum single pulse S/N and the single pulse widths covered by their search (starting from the sampling time). We compute the sky temperature at each survey's central frequency with PYGSM. We use these values in the following equation from Cordes & McLaughlin (2003) to calculate pulse flux density:

$$S_{\mathrm{min,pulse}} = \frac{S/N_{\mathrm{min}} \times (T_{\mathrm{sys}} + T_{\mathrm{sky}}) \times \beta}{G \times \sqrt{n_{\mathrm{pol}} \times \Delta\nu \times w_{\mathrm{broadened}}}},$$

where $w_{\mathrm{broadened}}$ is the observed width of the transient signal. We calculate the broadened pulse width by taking into account sampling time and dispersion smearing. We assume a DM of 60 pc cm^{-3}. The surveys have all searched for single pulses to at least a 1000 pc cm^{-3}, thus a repeat FRB from the source of FRB 20210924D should have been detected if it had repeated during their observations (DM= 737 pc cm^{-3}). The limiting peak flux density for the single pulse search down to S/N=8 is $S_{\mathrm{pulse,1284\,MHz}} = 56$ mJy ms for an intrinsic pulse width of 1 ms at 60 pc cm^{-3}. The limiting fluence for the Sextans A GC is thus $S_{\mathrm{GC,pulse,1284\,MHz}} = 89$ mJy ms, for an intrinsic pulse width of 1 ms at 60 pc cm^{-3}. Again, this greatly improves the previous upper limit of 284 mJy ms for an intrinsic pulse width of 1 ms at 1352 MHz and 60 pc cm^{-3} (Burke-Spolaor et al. 2011).

6 DISCUSSION AND CONCLUSIONS

For a pulsar with a rotation period of 100 ms, our flux density sensitivity at 1400 MHz translates to a radio pseudo-luminosity[11] limit of $L_{\mathrm{pseudo,1400\,MHz}} = S_{1400\,\mathrm{MHz}} \times D^2 = 7.9\pm0.4$ Jy kpc^2, assuming an approximate distance to the galaxies of $D = 1375$ kpc (Tully et al. 2013; Bellazzini et al. 2014), and a power-law radio spectral index of -1.60 ± 0.54. According to the ATNF pulsar data base (Manchester et al. 2005), the highest pseudo-luminosity for a galactic pulsar is held by B1641−45 (also known as J1644−4559) with 6.1 Jy kpc^2 (Komesaroff et al. 1973; Jankowski et al. 2018). The highest pseudo-luminosity for an extragalactic pulsar is J0523−7125 in the LMC with 2.5 Jy kpc^2 (Wang et al. 2022). If the extreme high end of the pulsar luminosity distribution of the galaxies Sextans A and B extends slightly further than the Milky Way's and above our limit, no such bright pulsars are beamed in our direction and were unobscured during our observations (e.g. due to excessive DM, scattering, or eclipsing), as we have observed the entire dwarf galaxies. However, the beaming fraction of pulsars is estimated to be around 20 per cent (Taylor & Manchester 1977), though newer surveys may alter this value (e.g. Turner et al. 2024).

As shown in Fig. 9, we could not detect any single pulses from known rapidly rotating radio transients or giant pulses (GPs) from known pulsars if they were situated at the distance of the Sextans galaxies and beamed in our direction–including the extragalactic Crab analogue PSR B0540−6919 (Seward et al. 1984; Johnston & Romani 2003). We could not detect very short time-scale pulses either as our time resolution was too large in the transient search (306 μs). However, we could detect FRB-like single pulses, similar to those seen from the Galactic magnetar SGR 1935+2154 (Bochenek et al. 2020; The CHIME/FRB Collaboration 2020). As stated in Section 1, the presence of magnetars in Sextans A and B is made more likely by the recent star formation in these galaxies. From our search, we conclude that no FRBs or FRB-like events from Sextans A or B were beamed in our direction at the time of observing. We did detect a new FRB in the incoherent and a number of (widely spaced) coherent beams of one of the Sextans A observations, but we were not able to constrain its sky position. We believe it is not associated with the dwarf galaxy due to its S/N being strongest in the incoherent beam. All detections in the coherent beams, which were covering the entire galaxy, are consistent with being detected via sidelobes. We can assume the sum of the Milky Way (see Section 1) and Intergalactic Medium DM contributions is of the order of 50 pc cm^{-3} at the redshift of Sextans A ($z_{\mathrm{Sextans}} \simeq 3 \times 10^{-4}$), using the Macquart relation (Macquart et al. 2020). We are thus left with 687 pc cm^{-3} to account for, which are unlikely to be attributed to the tenuous Sextans A galaxy content, but rather a much more distant

[11]This is an approximation of the pulsar luminosity using a flux density and distance approximation.

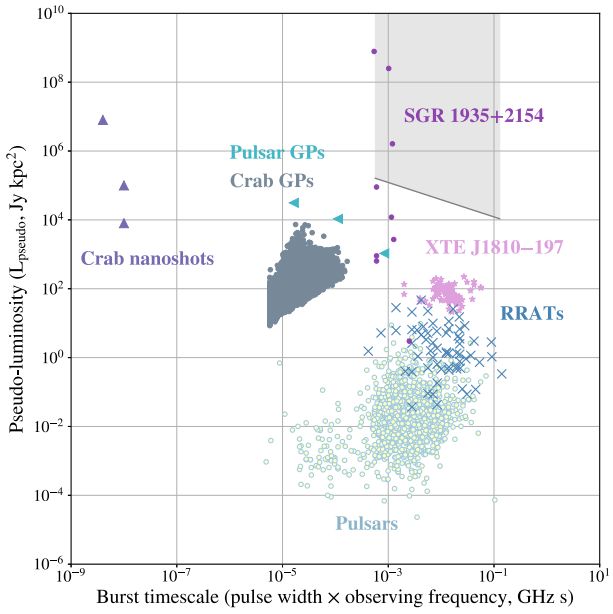

Figure 9. Pseudo-luminosity versus burst time-scale of radio bursts from NSs. The sensitivity of our survey of the Sextans A galaxy is shaded in grey. The Sextans B observations yield similar results. GPs and regular pulses from pulsars and rapidly rotating radio transients, as well as bursts from two magnetars, XTE J1810−197 and SGR 1935+2154, are depicted. Data and figure courtesy of Manisha Caleb, adapted from Driessen et al. (2023), originally from Pietka, Fender & Keane (2015). The source code of this figure is available on this GitHub repository.

galaxy host at an expected redshift of $z_{host} \simeq 0.6$. This new transient, FRB 20210924D, is not, to our knowledge, a known repeater despite being visible to CHIME (The CHIME/FRB Collaboration 2018).

ACKNOWLEDGEMENTS

The MeerKAT telescope is operated by the South African Radio Astronomy Observatory, which is a facility of the National Research Foundation, an agency of the Department of Science and Innovation. SARAO acknowledges the ongoing advice and calibration of GPS systems by the National Metrology Institute of South Africa (NMISA) and the time space reference systems department of the Paris Observatory.

TRAPUM observations used the FBFUSE and APSUSE computing clusters for data acquisition, storage, and analysis. These clusters were funded and installed by the Max-Planck-Institut für Radioastronomie and the Max-PlanckGesellschaft.

EC acknowledges funding from the United Kingdom's Research and Innovation Science and Technology Facilities Council (STFC) Doctoral Training Partnership, project reference 2487536.

AP and MB acknowledge that part of this work has been funded using resources from the INAF Large Grant 2022 'GCjewels' (P.I. Andrea Possenti) approved with the Presidential Decree 30/2022.

EB, MK, PVP, and VVK acknowledge continuing support from the Max Planck Society.

RPB acknowledges support from the ERC under the European Union's Horizon 2020 research and innovation programme (grant agreement No. 715051; Spiders).

We acknowledge the use of NASA's *SkyView* facility (http://skyview.gsfc.nasa.gov) located at NASA Goddard Space Flight Center to access the Digitized Sky Survey images of Sextans A and B. The Digitized Sky Survey was produced at the Space Telescope Science Institute under U.S. Government grant NAG W-2166. The images of these surveys are based on photographic data obtained using the Oschin Schmidt Telescope on Palomar Mountain and the UK Schmidt Telescope. The plates were processed into the present compressed digital form with the permission of these institutions.

This research made use of APLPY, an open-source plotting package for Python (Robitaille & Bressert 2012).

This research has made use of the SIMBAD data base, operated at CDS, Strasbourg, France (Wenger et al. 2000). This research has made use of NASA's Astrophysics Data System Bibliographic Services and the FRBSTATS catalogue.

This paper has made use of the ATNF pulsar catalogue version 1.69.

DATA AVAILABILITY

The data underlying this article will be shared upon reasonable request to the TRAPUM collaboration. The first and second pass observations were stored in a reduced resolution format only, cleaned by IQRM. The resolution was decreased to 512 channels and a 1.225 ms sampling time. The raw data of all pointings were deleted immediately after processing as they were too large to store. All secondary processing data products were retained for possible future inspection, including candidates which can be readily shared with interested observers.

REFERENCES

Asad K. M. B. et al., 2021, MNRAS, 502, 2970
Bailes M. et al., 2020, Publ. Astron. Soc. Aust., 37, e028
Barr E. D., 2020, Astrophysics Source Code Library, record ascl:2001.014
Barsdell B. R., Bailes M., Barnes D. G., Fluke C. J., 2012, MNRAS, 422, 379
Beasley M. A., Leaman R., Gallart C., Larsen S. S., Battaglia G., Monelli M., Pedreros M. H., 2019, MNRAS, 487, 1986
Bellazzini M. et al., 2014, A&A, 566, A44
Bhardwaj M. et al., 2021, ApJ, 910, L18
Bochenek C. D., Ravi V., Belov K. V., Hallinan G., Kocz J., Kulkarni S. R., McKenna D. L., 2020, Nature, 587, 59
Boyles J. et al., 2013, ApJ, 763, 80
Burgay M. et al., 2006, MNRAS, 368, 283
Burke-Spolaor S. et al., 2011, MNRAS, 416, 2465
Carli E., Levin L., Stappers B. W., Barr E. D., 2024, MNRAS, 531, 2835
Chen W., Barr E., Karuppusamy R., Kramer M., Stappers B., 2021, J. Astron. Instr., 10, 2150013
Cordes J. M., Lazio T. J. W., 2004, in Clemens D., Shah R. Y., Brainerd T.eds, ASP Conf. Ser. Vol. 317, Milky Way Surveys: The Structure and Evolution of Our Galaxy. Astron. Soc. Pac., San Francisco, p. 21
Cordes J. M., McLaughlin M. A., 2003, ApJ, 596, 1142
Dalcanton J. J. et al., 2009, ApJS, 183, 67
Dohm-Palmer R. C. et al., 1997, AJ, 114, 2527
Driessen L. N. et al., 2023, MNRAS, 527, 3659
Esposito P., Rea N., Israel G. L., 2021, Timing Neutron Stars: Pulsations, Oscillations and Explosions. Springer, Berlin, Heidelberg, p. 97
Garcia M., Herrero A., Najarro F., Camacho I., Lorenzo M., 2019, MNRAS, 484, 422
Gerasimov I. S., Egorov O. V., Lozinskaya T. A., Moiseev A. V., Oparin D. V., 2022, MNRAS, 517, 4968
Gerasimov I. S., Egorov O. V., Moiseev A. V., Kniazev A. Y., Lozinskaya T. A., Egorova E. S., 2024, MNRAS, 529, 1138
Gvozdenko A., Larsen S. S., Beasley M. A., Cabrera-Ziri I., Eitner P., Battaglia G., Leaman R., 2024, A&A, 685, A154
Haberl F., Sturm R., 2016, A&A, 586, A81
Harris J., Zaritsky D., 2004, AJ, 127, 1531

Harris J., Zaritsky D., 2009, AJ, 138, 1243
Hayden M. R. et al., 2014, AJ, 147, 116
Heger A., Fryer C. L., Woosley S. E., Langer N., Hartmann D. H., 2003, ApJ, 591, 288
Helfand D. J., Long K. S., 1979, Nature, 282, 589
Hisano S. et al., 2022, ApJ, 928, 161
Jankowski F., 2022, Astrophysics Source Code Library, record ascl:2208.003
Jankowski F., van Straten W., Keane E. F., Bailes M., Barr E. D., Johnston S., Kerr M., 2018, MNRAS, 473, 4436
Jankowski F. et al., 2023, MNRAS, 524, 4275
Johnston H. M., Kulkarni S. R., 1991, ApJ, 368, 504
Johnston S., Romani R. W., 2003, ApJ, 590, L95
Kappes M., 2005, PhD thesis, Rheinische Friedrich-Wilhelms-Universität Bonn
Karachentsev I. D., Karachentseva V. E., Huchtmeier W. K., Makarov D. I., 2004, AJ, 127, 2031
Keane E. F. et al., 2018, MNRAS, 473, 116
Keith M. J. et al., 2010, MNRAS, 409, 619
Kirsten F. et al., 2022, Nature, 602, 585
Komesaroff M. M., Ables J. G., Cooke D. J., Hamilton P. A., McCulloch P. M., 1973, ApJ, 15, L169
Kouwenhoven M. L. A., Voûte J. L. L., 2001, A&A, 378, 700
Kremer K., Li D., Lu W., Piro A. L., Zhang B., 2023, ApJ, 944, 6
Lamb R. C., Fox D. W., Macomb D. J., Prince T. A., 2002, ApJ, 574, L29
Levin L., 2012, PhD thesis, Swinburne Univ. Technology
Lewandowski W., Kowalińska M., Kijak J., 2015, MNRAS, 449, 1570
Lorenzo M., Garcia M., Najarro F., Herrero A., Cerviño M., Castro N., 2022, MNRAS, 516, 4164
Lorimer D. R., 2008, Living Rev. Relativ., 11, 8
Lorimer D. R., Kramer M., 2005, Handbook of Pulsar Astronomy. Cambridge Univ. Press, Cambridge
Luck R. E., Moffett T. J., Barnes III T. G., Gieren W. P., 1998, AJ, 115, 605
Lynch R. S. et al., 2013, ApJ, 763, 81
Macquart J.-P. P. et al., 2020, Nature, 581, 391
Maggi P. et al., 2019, A&A, 631, A127
Maitra C., Esposito P., Tiengo A., Ballet J., Haberl F., Dai S., Filipović M. D., Pilia M., 2021, MNRAS, 507, L1
Manchester R. N. et al., 1996, MNRAS, 279, 1235
Manchester R. et al., 2001, MNRAS, 328, 17
Manchester R. N., Hobbs G. B., Teoh A., Hobbs M., 2005, AJ, 129, 1993
Men Y., Barr E., 2024, A&A, 683, A183
Men Y., Barr E., Clark C. J., Carli E., Desvignes G., 2023, A&A, 679, A20
Mereghetti S. et al., 2024, Nature, 629, 58
Mohan N., Rafferty D., 2015, Astrophysics Source Code Library, record ascl:1502.007
Morello V., 2023, Astrophysics Source Code Library, record ascl:2310.008
Morello V. et al., 2019, MNRAS, 483, 3673
Morello V., Rajwade K. M., Stappers B. W., 2021, MNRAS, 510, 1393
Obrocka M. K., 2015, PhD thesis, Univ. Manchester
Padmanabh P. V. et al., 2023, MNRAS, 524, 1291
Paturel G., Petit C., Prugniel P., Theureau G., Rousseau J., Brouty M., Dubois P., Cambrésy L., 2003, A&A, 412, 45
Pietka M., Fender R. P., Keane E. F., 2015, MNRAS, 446, 3687
Platts E., Weltman A., Walters A., Tendulkar S., Gordin J., Kandhai S., 2019, Phys. Rep., 821, 1
Price D. C., 2016, Astrophysics Source Code Library, record ascl:1603.013
Rajwade K. M. et al., 2022, MNRAS, 514, 1961
Rane A., Lorimer D. R., Bates S. D., McMann N., McLaughlin M. A., Rajwade K., 2016, MNRAS, 455, 2207
Robitaille T., Bressert E., 2012, Astrophysics Source Code Library, record ascl:1208.017
Sakai S., Madore B. F., Freedman W. L., 1997, ApJ, 480, 589
Sengar R. et al., 2023, MNRAS, 522, 1071
Seward F. D., Harnden F. R. J., Helfand D. J., 1984, ApJ, 287, L19
Sharina M. E., Puzia T. H., Krylatyh A. S., 2007, Astrophys. Bull., 62, 209
Space Telescope Science Institute, 1995, The Digitized Sky Survey. Infrared Processing and Analysis Centre, Pasadena, California
Stappers B., Kramer M., 2016, in Proceedings of MeerKAT Science: On the Pathway to the SKA – PoS(MeerKAT2016). Sissa Medialab, Trieste Italy, p. 009
Taylor J. H., Huguenin G. R., 1969, Nature, 221, 816
Taylor J. H., Manchester R. N., 1977, ApJ, 215, 885
Tendulkar S. P. et al., 2017, ApJ, 834, L7
The CASA Team, 2022, PASP, 134, 114501
The CHIME/FRB Collaboration, 2018, ApJ, 863, 48
The CHIME/FRB Collaboration, 2020, Nature, 587, 54
Titus N., Stappers B. W., Morello V., Caleb M., Filipović M. D., McBride V. A., Ho W. C. G., Buckley D. A. H., 2019, MNRAS, 487, 4332
Titus N., Toonen S., McBride V. A., Stappers B. W., Buckley D. A. H., Levin L., 2020, MNRAS, 494, 500
Trigg A. C. et al., 2024, A&A, 687, A173
Tully R. B. et al., 2013, AJ, 146, 86
Turner J. D. et al., 2024, MNRAS, 531, 3579
Wang Y. et al., 2022, ApJ, 930, 38
Weisz D. R. et al., 2011, ApJ, 739, 5
Wenger M. et al., 2000, A&AS, 143, 9
Xu H. et al., 2022, Nature, 609, 685
Yang J., Laycock S. G. T., Christodoulou D. M., Fingerman S., Coe M. J., Drake J. J., 2017, ApJ, 839, 119
Yao J. M., Manchester R. N., Wang N., 2017, ApJ, 835, 29
Zheng H. et al., 2017, MNRAS, 464, 3486
Zhu W. W. et al., 2014, ApJ, 781, 117

This paper has been typeset from a TEX/LATEX file prepared by the author.